Applied and Environmental Microbiology

# Rumen *Lachnospiraceae* isolate NK3A20 exhibits metabolic flexibility in response to substrate and coculture with a methanogen

Rachel A. Kaminsky,[1] Peter M. Reid,[1] Eric Altermann,[2,3] Nikki Kenters,[1] William J. Kelly,[1] Samantha J. Noel,[1] Graeme T. Attwood,[1] Peter H. Janssen[1]

**AUTHOR AFFILIATIONS** See affiliation list on p. 14.

**ABSTRACT** Hydrogen ($H_2$) is the primary electron donor for methane formation in ruminants, but the $H_2$-producing organisms involved are largely uncharacterized. This work integrated studies of microbial physiology and genomics to characterize rumen bacterial isolate NK3A20 of the family *Lachnospiraceae*. Isolate NK3A20 was the first recognized isolate of the NK3A20 group, which is among the ten most abundant bacterial genera in 16S rRNA gene surveys of rumen microbiota. NK3A20 produced acetate, butyrate, $H_2$, and formate from glucose. The end product ratios varied when grown with different substrates and at different $H_2$ partial pressures. NK3A20 produced butyrate as a major product using glucose or under high $H_2$ partial pressures and switched to mainly acetate in the presence of galacturonic acid (an oxidized sugar) or in coculture with a methanogen. Growth with galacturonic acid was faster at elevated $H_2$ concentrations, while elevated $H_2$ slowed growth with glucose. Genome analyses revealed the presence of multiple hydrogenases including a membrane-bound Ech hydrogenase, an electron bifurcating butyryl-CoA dehydrogenase (Bcd-Etf), and an Rnf complex that may be involved in modulating the observed metabolic pathway changes, providing insight into $H_2$ formation in the rumen.

**IMPORTANCE** The genus-level NK3A20 group is one of the ten most abundant genera of rumen bacteria. Like most of the rumen bacteria that produce the hydrogen that is converted to methane in the rumen, it is understudied, without any previously characterized isolates. We investigated isolate NK3A20, a cultured member of this genus, and showed that it modulates hydrogen production in response to its growth substrates and the hydrogen concentration in its environment. Low-hydrogen concentrations stimulated hydrogen formation, while high concentrations inhibited its formation and shifted the fermentation to more reduced organic acid products. We found that growth on uronic acids, components of certain plant polymers, resulted in low hydrogen yields compared to glucose, which could aid in the selection of low-methane feeds. A better understanding of the major genera that produce hydrogen in the rumen is part of developing strategies to mitigate biogenic methane emitted by livestock agriculture.

**KEYWORDS** hydrogen, methane, rumen bacteria, interspecies hydrogen transfer, butyrate, uronic acids

The rumen houses a genetically and functionally diverse microbiome that mediates ruminant host nutrition through fermentation end products and is, in turn, influenced by the host's diet (1, 2). Methane ($CH_4$) is generated by methanogenic archaea in the rumen microbial community and represents a potential loss of energy to the host (3). $CH_4$ produced by farmed ruminants also contributes to anthropogenic greenhouse

gas emissions (4). Most rumen methanogens use hydrogen gas ($H_2$) as a substrate for methanogenesis, which is produced from carbohydrate fermentation by rumen bacteria, protozoa, and fungi (5). Known as interspecies $H_2$ transfer, this interaction is thought to be integral to ruminal $CH_4$ emissions and controlling rumen fermentation through $H_2$ removal (6, 7). The rumen celluloytic bacterium *Ruminococcus albus* serves as a model species for studies of interspecies $H_2$ transfer, where the consumption of $H_2$ by a hydrogenotroph facilitates more $H_2$ formation than in the absence of the $H_2$-using partner (8–12). Other rumen organisms that display this behavior include *Ruminococcus flavefaciens* (13), *Selenomonas ruminantium* (14), and several fungi (15, 16), indicating that this is an important function in gut ecosystems. It is known that many ruminal bacterial genomes encode hydrogenases, indicating a prevalent capability to produce $H_2$ (12). Identification and investigation of these species and their potential to participate in interspecies $H_2$ transfer may be an important step toward understanding $CH_4$ production and mitigating emissions.

The family *Lachnospiraceae* is abundant in gut environments and comprises part of the core rumen microbiome (2, 17). Several poorly studied *Lachnospiraceae*-associated lineages are posited to possess hydrogenases (12, 18). Studies on cultured lineages, including members of *Butyrivibrio* and *Roseburia*, indicate that polysaccharide degradation and butyrate production are key characteristics of members of *Lachnospiraceae* (19). Molecular studies have uncovered significant genetic and potential functional diversity within this family (20), but there remain many uncharacterized *Lachnospiraceae* genera of interest to rumen microbiology (17, 21).

This study characterized the novel rumen bacterial isolate NK3A20. It is a member of the family *Lachnospiraceae* and the first cultured representative of the NK3A20 group. The NK3A20 group probably represents a genus-level taxonomic group and is commonly found among the most abundant taxa in surveys of gut microbiota (21, 22). For example, Henderson and colleagues estimated that this probable genus constitutes 2.7% of rumen bacteria and was the seventh most abundant ruminal bacterial genus in the Global Rumen Census (2, 21). We studied the metabolism of isolate NK3A20 to better understand this otherwise unstudied group. In particular, we were interested in the range of substrates this bacterium can use for growth and its potential role in $H_2$ formation as a precursor of $CH_4$ generation in the rumen. A better understanding of the major genera that produce $H_2$ in the rumen is part of developing strategies to mitigate biogenic $CH_4$ emitted by livestock agriculture.

## MATERIALS AND METHODS

### Sources of strains

NK3A20 was isolated from rumen contents from a sheep grazing rye-grass-dominated pasture in the Manawatū region of New Zealand (23). Isolation was through a dilution-to-extinction approach (23, 24) in RM02 liquid medium supplemented with glucose, cellobiose, xylose, L-arabinose, casamino acids, Bacto-peptone, and yeast extract (23). *Methanobrevibacter olleyae* strain 1H5-1P (DSM 16632; 25) was purchased from DSMZ (Braunschweig, Germany).

Strain purity was assessed by microscopy of Gram stained (26) and wet mount preparations and by 16S rRNA gene sequencing, using the methods described in reference (23).

### Microscopy

Phase contrast photomicrographs were taken using a DM2500 microscope (Leica Microsystems, Wetzlar, Germany) with a 100× oil phase contrast objective, and the images were captured digitally using Leica Application Suite software. Cell dimensions were calculated using imaging software and parallel photomicrographs of a reference stage micrometer.

## Cultures and growth conditions

Cultures were revived from frozen stocks (−80°C; AgResearch Rumen Microbiology collection) in Hungate tubes (Bellco Glass, Vineland, NJ, USA) containing 9 mL of RM02 medium (23) under a 100% $CO_2$ headspace (BOC Gas, Palmerston North, New Zealand). Bacterial cultures were supplemented with 0.5 mL 2× GenRFV, a stock solution containing a mix of substrates and vitamins dissolved in clarified rumen fluid. This was modified from GenRFV described in reference (23) to contain stock concentrations of 40 mM each for glucose and xylose and 20 mM each for cellobiose and arabinose or twice that in the original recipe.

Methanogen cultures were supplemented with 0.5 mL clarified rumen fluid (23) containing 4 mM $CaCl_2$, 3 mM $MgCl_2$, 2% (wt/vol) yeast extract, and vitamins (NoSubRFV; final concentrations). Cultures were also supplemented with 60 mM sodium formate and 20 mM sodium acetate (final concentrations; added as 0.2 mL from a concentrated stock). Supplements were filtered directly into tubes using sterile 0.22 µm pore size Millex GP filters (Millipore Corp., Bedford, MA, USA) fitted to sterile plastic syringes and needles (Becton Dickinson and Co., Franklin Lakes, NJ, USA). Methanogen cultures were pressurized with $H_2$: $CO_2$ (80:20 vol/vol) to 140 kPa over the 101 kPa $CO_2$ already in the tubes. Tubes were closed with butyl rubber stoppers and screw caps (Bellco Glass).

All cultures were incubated at 39°C and in the dark. Cultures were incubated statically for growth substrate tests. Cultures in growth kinetics and coculture experiments were shaken horizontally on an Orbitex XL orbiting platform (Infors HT, Basel, Switzerland) set to 50 rpm. It should be noted that comparisons of results between static and shaken experiments could be confounded by differences in the conditions.

## Measuring culture density

Optical density was measured at 600 nm either by inserting Hungate tubes directly into a Spectronic 200 spectrophotometer (ThermoFisher Scientific, Auckland, New Zealand) or by taking samples using disposable 1 mL plastic syringes and needles and measuring the optical density in disposable 1 cm path length semi-micro polystyrene cuvettes (Greiner Bio-One, Kremsmünster, Austria). Absorbance was set to zero using water, and the optical density measurements were corrected for uninoculated medium, or the absorbance was set to zero using tubes containing uninoculated medium.

## Testing use of growth substrates

Individual substrates were sterilized by autoclaving them separately as concentrated stocks or suspensions and then added to Hungate tubes containing RM02 medium supplemented with NoSubRFV (1% vol/vol). Final concentrations of substrates were 20 mM for organic acids, 10 mM for monosaccharides, 5 mM for disaccharides, or 0.2% (wt/vol) for polysaccharides, unless noted otherwise. Amorphous cellulose was prepared using the method described in reference (27). Acids were added as their sodium salts.

To measure growth on different substrates, a 1% (vol/vol) inoculum was added to triplicate Balch tubes (Bellco Glass) each containing 9 mL of RM02 medium, 0.5 mL NoSubRFV, and 5 or 10 mM of a single substrate (final concentration) added in 0.2 mL of a concentrated solution, with a headspace of 100% $CO_2$. Vials were closed with butyl rubber stoppers (Fit Prototyping, Lupburg, Germany) and aluminum caps (Bellco Glass).

## Growth kinetics

To assess growth and end-product accumulation, a 1% (vol/vol) inoculum was added to triplicate 125 mL serum vials (Bellco Glass) each containing 46 mL of RM02 medium, 2.5 mL NoSubRFV, and either 10 mM glucose or 10 mM sodium galacturonic acid (final concentrations) added from a concentrated solution at 0.5 mL per vial. Vials were closed with butyl rubber stoppers (Fit Prototyping) and aluminum caps (Bellco Glass) with a headspace of 100% $CO_2$. Cultures were shaken during incubation.

## Coculture experiment

*M. olleyae* was grown in Hungate tubes (5% vol/vol inoculum) under the methanogen culture conditions described above. Cultures were grown to stationary phase to ensure that there was sufficient methanogen cell mass. Culture headspaces were then flushed free of $CH_4$ and any residual $H_2$ with 100% $CO_2$, before 10 mM glucose or sodium galacturonic acid was added in 0.2 mL from concentrated stocks. NK3A20 was inoculated at 1% (vol/vol). Concurrent pure cultures of NK3A20 were grown with 9 mL RM02 medium and 0.5 mL NoSubRFV and supplemented with the same substrates as cocultures. Half of the bacterial pure cultures were pressurized with $H_2$: $CO_2$ (80:20 vol/vol) to 140 kPa over the 101 kPa $CO_2$ already in the tubes, while the other half remained under 100% $CO_2$.

## Fermentation end-product analysis

$H_2$ and $CH_4$ concentrations in the gas headspace were measured by taking a 0.5 mL headspace sample at the pressure in the culture vessel. Samples were taken using polycarbonate 1 mL Luer-Lok syringes (Becton Dickinson and Co., Franklin Lakes, NJ, USA) fitted with Mininert Luer-tip syringe valves (Hamilton, Reno, NV, USA). Samples were manually injected into an Aerograph 660 gas chromatograph (Varian Associates, Palo Alto, CA, USA) fitted with a Porapak Q80/100 mesh column (Waters Corporation, Milford, MA, USA) and a thermal conductivity detector. Nitrogen ($N_2$) was used as the carrier gas. A standard containing 5%:30%:65% vol/vol/vol $H_2$:$CH_4$:$N_2$ (BOC Gas, Palmerston North, NZ) was measured using a 0.5 mL sample at 1 atm for calibration. This standard was also diluted in 100% $N_2$ to give 0.03% $H_2$ for the detection of low concentrations. Dissolved $H_2$ concentrations were calculated from the headspace concentrations using Ostwald coefficients tabulated by reference (28) and molar gas volumes from reference (29), assuming that the headspace gases were in equilibrium with the dissolved gases. $H_2$ and $CH_4$ formation are reported as amounts per liter of culture, even though they accumulate in the gas phase of the culture vessels and include both gaseous and dissolved fractions, unless noted otherwise.

Liquid cultures were sampled (1 mL) into 1.5 mL tubes (Axygen, Inc., Union City, CA, USA) for fermentation product analysis. Samples were centrifuged (13,000 × *g* for 13 min) in a benchtop centrifuge (Eppendorf, Hamburg, Germany). 900 µL of supernatant was collected into a clean 1.5 mL tube, and 100 µL of internal standard (20 mM ethylbutyrate in 20% wt/vol $H_3PO_4$) was added. Samples were stored at −20°C until analyzed for a minimum of 24 hours.

Samples were thawed and centrifuged (13,000 × *g* for 13 min), and 800 µL of supernatant was collected into a crimp-capped GC vial (ThermoFisher Scientific) for alcohol and aqueous short-chain fatty acid analysis. Vials were stored at 4°C until analysis. The remaining 200 µL supernatant was collected into 1.5 mL tubes (Eppendorf, Hamburg, Germany) for derivatized organic acid analysis.

Analysis of alcohols (methanol, ethanol, 1-propanol, and 1-butanol) and aqueous short-chain fatty acids (acetate, propionate, butyrate, isobutyrate, 2-methylbutyrate, valerate, isovalerate, and caproate) was performed using a GC-2010 Plus equipped with an AOC 20i auto injector (Shimadzu Corporation, Kyoto, Japan), a Zebron ZB-FFAP Capillary GC Column (Phenomenex, Torrence, CA, USA), and helium carrier gas (BOC Gas). The injection temperature was 90°C, and the FID detector temperature was 240°C. The GC column temperature was set to 60°C for 3.5 min, then increased to 120°C (at 30°C/min), then to 185°C (10°C/min), and lastly to 200°C (at 15°C/min) with a final 3-min hold.

Samples were derivatized using a downscaled method described in reference (30). Briefly, 5 µL of 1% (wt/vol) resazurin dye, 100 µL of 37% (wt/vol) HCl, and 800 µL diethyl-ether were added to a 1.5 mL tube containing 200 µL of sample. Samples were shaken vigorously then left to settle for 1 minute. The top ether layer was collected into a new 2 mL tube. The previous step was repeated, and the ether layer was

collected again and added to the same tube. 100 µL of derivatization agent (*N*-methyl-*N*-t-butyldemetzylsilytriflouroacetamide; ThermoFisher Scientific) and 800 µL of ether layer were added to a GC vial. Vials were crimp capped immediately with aluminum caps. Samples were heated at 80°C for 20 min and left under a fume hood for 48 hours before analysis. Analysis of derivatized organic acids (formate, lactate, and succinate) was performed using a GC-2010 Plus equipped with a Barrier Ionization Discharge (BID) detector, AOC 6000 auto-sampler, VICI heated helium purifier (Valco Instruments Co. Inc. Houston, TX, USA), Zebron ZB-5MS Capilliary GC Column, and helium carrier gas. The GC conditions were as follows: 1 µL of sample split injection (20:1 split ratio), injection temperature set to 240°C, BID detector temperature set to 250°C, GC column temperature set to 50°C for 2 min, then increased to 130°C (at 5°C/min), and then to 240°C (at 15°C/min) with a final 4.67-min hold.

The amounts of each analyte were quantified using LabSolutions software (Shimadzu Corporation, Kyoto, Japan) by comparing the peak area of each analyte to its corresponding standard curve.

Carbon and available $H_2$ balances were calculated as described in reference (31). Statistics and graphs were generated using RStudio (32) using the ggplot2 (33), reshape2 (34), plyr (35), and viridis (36) packages.

## Phylogenetic analyses

The 16S rRNA gene sequence of NK3A20 was aligned with type strain sequences from the family *Lachnospiraceae* as found in the LPSN - List of Prokaryotic names with Standing in Nomenclature (37). Only species with 16S rRNA sequences (≥ 1,371 nt) available in GenBank were included. Alignments were performed using ClustalW implemented in MEGA (version 10.0.50; 38). A phylogenetic tree was reconstructed in MEGA using the maximum-likelihood method and Jukes-Cantor model (39) with 1,000 bootstrap iterations.

## Genome analyses

The resources available from JGI's Integrated Microbial Genomes and Microbiome Samples (IMG/M) database were used for genome sequence analysis (40). Annotations were performed using GAMOLA2 (41) and visualized in a customized version of the Artemis Genome Viewer (version 16) (42). Annotations were also generated using the BlastKoala function and mapped to pathways in KEGG (43). Hydrogenases were identified and categorized using HydDB (44).

## RESULTS AND DISCUSSION

### Cell morphology

Cells of isolate NK3A20 stained Gram negative and were non-motile. Cells were ovals with pointed ends, averaging 1.6 µm long and 0.82 µm in diameter (SD = 0.23 and 0.22, respectively; *n* = 100), and were often in pairs or chains (Fig. 1). Division appeared to be by binary fission.

### Phylogenetic placement

A phylogenetic comparison of 16S rRNA genes from NK3A20 and those of type strains from *Lachnospiraceae* indicated that this isolate forms a distinct lineage in the tree and probably represents a novel genus (Fig. S1). The closest relative of NK3A20 was *Butyrivibrio proteoclasticus* (88.82% sequence identity). 16S rRNA gene sequence identities of <96% are usually considered to indicate membership of distinct genera (45, 46). In the Genome Taxonomy Database (GTDB release 214, 28 April 2023; 47), strain NK3A20 is classified in genus CAG-791, as species sp900107575. NK3A20 has also been assigned the name *Candidatus* Efretella ranebella based on its genome (48).

FIG 1 Phase contrast photomicrograph of cells of NK3A20. The scale bar represents a distance of 10 µm.

## Substrates supporting growth

NK3A20 was tested for its ability to grow using 28 different carbon and energy sources. Good growth ($OD_{600}$ >0.7) was supported by a range of sugars (Table 1). Soluble sugars and uronic acids supported good growth of NK3A20, but polysaccharides did not.

## Genome analysis of carbohydrate metabolism

Examination of the genome sequences revealed that NK3A20 had an extensive complement of glycosyl hydrolases (83 from 28 families; Table S1). Many of these families include enzymes able to cleave galactoside (GH2, GH35, GH36, GH42, and GH53) and arabinoside/xyloside (GH5, GH8, GH10, GH11, GH30, GH39, GH43, GH120, and GH127) linkages. NK3A20 was unable to initiate the breakdown of most plant polysaccharides, suggesting that few of the carbohydrate-degrading enzymes are secreted from the cell.

Most of the carbohydrate-degrading enzymes are predicted to be intracellular, suggesting that NK3A20 can transport a variety of oligosaccharides into the cell, where they are further metabolized. This is supported by the diversity of carbohydrate transporters found in the genome (Table S2). The genome had >20 genes encoding proteins from functional category COG1653 that includes proteins predicted to transport oligosaccharides. A small number of GHs have signal peptides (Table S1). These were found only in members of the GH3, GH10, GH11, GH13, and GH25 families. The GH10 and GH11 are presumably secreted xylanases and GH13 enzymes degrade starch and similar carbohydrates. GH3 can have a range of functions including involvement in bacterial cell wall modification, and GH25 are lysozymes that also have a role in bacterial cell wall degradation. It is also apparent that NK3A20 has very few carbohydrate-binding domains associated with the GHs. *Lachnospiraceae* are generally thought to contribute to fibrolytic activity (19, 49, 50), but NK3A20 can be seen as a secondary carbohydrate

**TABLE 1** Substrates supporting growth of NK3A20[a]

| Substrate (concentration tested)[b] | Growth[c] |
|---|---|
| No substrate added | − |
| Raffinose (5 mM) | ++ |
| Cellobiose (5 mM) | ++ |
| Melibiose (5 mM) | ++ |
| Sucrose (5 mM) | ++ |
| Lactose (5 mM) | ++ |
| Maltose (5 mM) | ++ |
| Glucose (10 mM) | ++ |
| Fructose (10 mM) | + |
| Galactose (10 mM) | ++ |
| Arabinose (10 mM) | ++ |
| Rhamnose (10 mM) | − |
| Xylose (10 mM) | ++ |
| Mannose (10 mM) | ++ |
| Ribose (10 mM) | − |
| Fucose (10 mM) | − |
| Sorbose (10 mM) | − |
| Lactate (20 mM) | − |
| Succinate (20 mM) | − |
| Galacturonate (20 mM) | ++ |
| Glucuronate (20 mM) | ++ |
| Pectin (0.1%) | + |
| Polygalacturonate (0.1%) | + |
| Starch (0.1%) | − |
| Amorphous cellulose (0.1%) | − |
| Crystalline cellulose (0.1%) | − |
| Inulin (0.1%) | − |
| Chitin (0.1%) | − |
| Xylan (0.1%) | + |

[a]Experiments were performed in Hungate tubes.
[b]All percentages are wt/vol.
[c]For simple sugars: ++, OD >0.3; +, OD >0.1; −, <0.1. For polymers: ++, >10 mmol/L total lactate, acetate, and butyrate; +, >1 mmol/L total lactate, acetate, and butyrate; −, products similar to those in control without added substrate.

degrader dependent on oligosaccharides or sugars generated by microbes able to initiate plant polysaccharide breakdown.

## Growth on different substrates

NK3A20 grew at different rates with different substrates, and the lag periods after transfer from a galacturonic acid-containing medium were sometimes long (Fig. 2). Maximum densities of cultures grown on xylose, galacturonic acid, and maltose were recorded within 36 hours, within 56 hours on lactose, and within 80 hours on glucose and galactose. There were differences in growth rate between replicate cultures growing on the same substrate, as indicated by the large error bars, particularly when the lags were longer. Growth *in situ* may not match these patterns as many sugars will be available at the same time, but these results may still aid in understanding factors that contribute to abundance trends of NK3A20 in microbiome studies and are important if this organism is used as a model for understanding rumen biology.

## End-product formation on different substrates

End-product generation was measured using increasing initial concentrations of glucose (Fig. 3). NK3A20 produced acetate and butyrate, small amounts of formate, and only
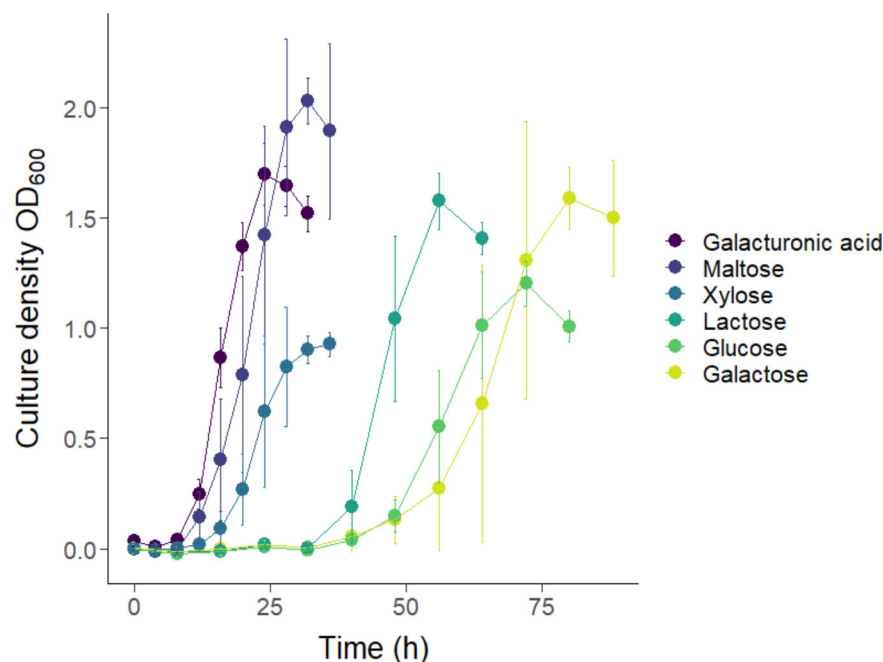
**FIG 2** Growth of isolate NK3A20 on different substrates initiated from the same galacturonic acid-grown inoculum in Balch tubes. Colors represent substrates. Error bars represent one SD from the mean of three (lactose only) or four replicates.

trace amounts of lactate and succinate (Fig. 3). $H_2$ gas also accumulated in the culture headspace. No methanol, ethanol, 1-propanol, 1-butanol, propionate, isobutyrate, 2-methylbutyrate, valerate, isovalerate, or caproate was produced after growth on glucose. End-product accumulation and culture density increased concomitantly with increasing substrate concentration up to about 10 mM initial glucose. End products did not change greatly in composition or proportion with different concentrations of glucose. Carbon recoveries and $H_2$ balances indicated that NK3A20 used all the substrate provided and that the major end products were accounted for (Table 2).

Substrates that supported good growth were tested for possible differences in end-product formation (Table S3). This revealed that the ratios of acetate and butyrate produced by NK3A20 varied depending on the substrate. Fermentation of hexoses and pentoses to pyruvate yields 2 NADH and 2 ATP, while fermentation of galacturonic acid and glucuronic acid (oxidized forms of galactose and glucose, respectively) to pyruvate yields no NADH and 1 ATP. This explains the dominance of acetate as a product from galacturonic acid and glucuronic acid fermentation (acetate: butyrate ratio of 2.74 and 2.83, respectively) because fewer electrons are available for butyrate formation, and acetate formation generates ATP while consuming no electrons. Hexoses and pentoses, and their dimers, yielded much smaller acetate: butyrate ratios, of 0.40 to 0.71, consistent with more electrons derived from the fermentation being routed to form the reduced fermentation product, butyrate.

**TABLE 2** End products, carbon recoveries, and available H balances of NK3A20 grown with 2.5 mM (25 µmol/tube) and 5 mM (50 µmol/tube) initial glucose

| Initial glucose (µmol/tube) | Products (µmol/tube)[a] | | | | | | | Carbon recovery | Available H balance |
|---|---|---|---|---|---|---|---|---|---|
| | Acetate | Butyrate | Formate | Succinate | Lactate | $H_2$ | $CO_2$[b] | | |
| 25 | 7.37 ± 5.05 | 17.90 ± 2.21 | 0.94 ± 0.26 | < 0.01 | 0.15 ± 0.26 | 66.37 ± 7.16 | 42.2 | 0.87 | 1.08 |
| 50 | 19.05 ± 1.69 | 37.92 ± 0.96 | 4.54 ± 0.47 | 0.55 ± 0.48 | 0.06 ± 0.10 | 123.27 ± 6.03 | 89.8 | 0.96 | 1.02 |

[a]The data are the means of three replicates ± SD.
[b]$CO_2$ produced during pyruvate conversion to acetyl-CoA was included in the carbon balance and was estimated by assuming two $CO_2$ are produced per butyrate and one per acetate. Formate and succinate were subtracted from the $CO_2$ estimate as one $CO_2$ is used to produce one formate or one succinate.
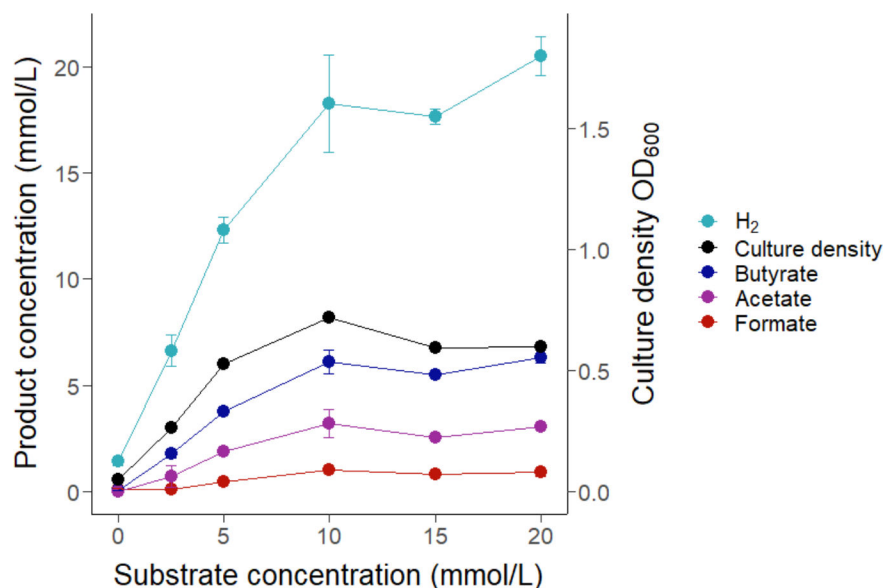
**FIG 3** Relationships between initial glucose concentration and end product formation by NK3A20. Experiments were performed in Hungate tubes. Colors represent measured growth indicators and end products. Error bars represent one SD from the mean from three replicates. Small amounts of lactate and succinate (<0.2 mmol/L) were detected (not shown).
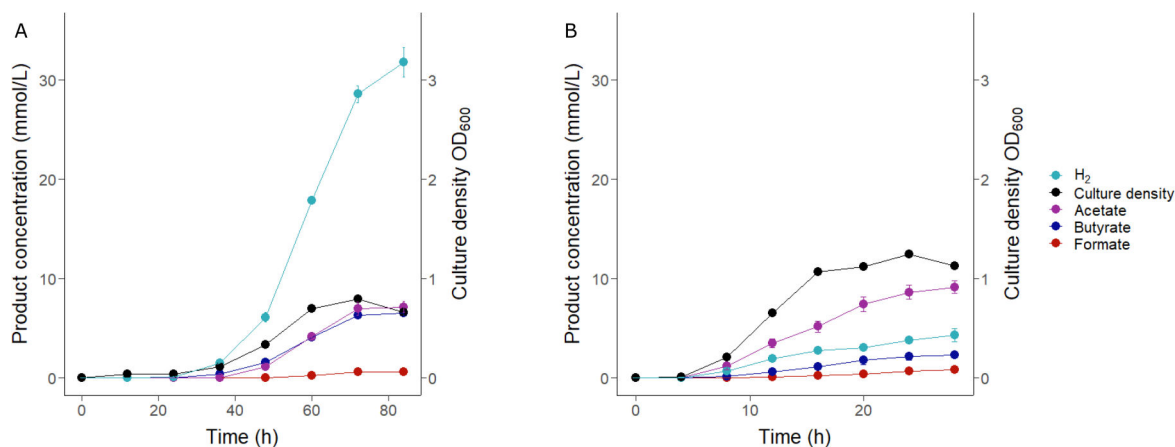
## Growth kinetics

Growth of NK3A20 was monitored to determine the generation of end products over time when grown with glucose (Fig. 4A) and galacturonic acid (Fig. 4B). End products accumulated concurrently with increases in optical density on both substrates.

The maximum optical density ($OD_{600}$) for NK3A20 growing with glucose was recorded 72 hours after inoculation, while maximum growth on galacturonic acid was recorded after 24 hours (Fig. 4A and B). The lag on glucose was long even with a glucose-grown inoculum, suggesting that galacturonic acid is a preferred substrate, as found previously (Fig. 2). The proportions of the products differed on the two substrates. With glucose, NK3A20 produced up to 32 mmol/L of $H_2$, 7 mmol/L of acetate, 7 mmol/L of butyrate, and 0.7 mmol/L formate. When grown with galacturonic acid, acetate was the major product, with up to 9 mmol/L produced, and less butyrate and $H_2$ were produced, as expected for this more oxidized sugar.

## Effect of $H_2$ on fermentation

Some studies have shown that fermentation product ratios of hydrogenogenic microbes shift when cocultured with a hydrogenotrophic microbe (e.g., 8, 13–16). We reduced the $H_2$ partial pressure by coculturing NK3A20 with *M. olleyae*, a methanogen that can use both $H_2$ and formate as energy sources. In addition, we added $H_2$ to pure cultures of NK3A20 prior to incubation to increase the initial dissolved $H_2$ partial pressure to about 600 µM, which is much greater than the 0.1 to 50 µM normally encountered by these organisms in the rumen (7).

The effects of $H_2$ use by the methanogen were tested in NK3A20 cultures supplemented with either glucose or galacturonic acid. $CH_4$ production was observed in the cocultures, and no formate or $H_2$ could be detected, indicating that any formate and $H_2$ produced by NK3A20 was consumed by *M. olleyae* (Table 3). Results clearly show shifts in the end products of NK3A20 in the presence of *M. olleyae*. $H_2$ and formate formation by the bacterium was assumed to be 4 mol per mol of $CH_4$ detected, and these are all reported as $H_2$. Production of acetate and $H_2$ from glucose fermentation by NK3A20 increased (Welch's two-sample *t*-test; acetate $P = 0.1$, $H_2$ $P = 0.002$), while

**FIG 4** Growth kinetics of NK3A20 on glucose (A) and galacturonic acid (B). Colors represent measured growth indicators and end products. The values are means from two (A) or three (B) replicates, and the error bars represent one SD from the mean. Experiments were performed in serum vials. Small amounts of succinate (<0.2 mmol/L) were detected in the cultures grown with galacturonic acid (not shown).

butyrate decreased ($P = 0.0006$) in coculture with the methanogen. When growing with galacturonic acid, acetate and $H_2$ increased (acetate $P = 0.06$, $H_2$ $P = 0.01$), while butyrate decreased ($P = 0.00007$). $CH_4$ formation was significantly lower from galacturonic acid (0.25 mol $CH_4$ per mol of sugar) than from glucose (0.6 mol $CH_4$ per mol of sugar; $P = 0.002$).

In contrast, results were reversed in pure cultures grown under increased partial pressures of $H_2$ (Table 3). Butyrate formation by NK3A20 increased (glucose $P = 0.06$, galacturonic acid $P = 0.0008$) while $H_2$ and acetate decreased on both substrates compared to pure culture controls without added $H_2$ ($H_2$ from glucose $P = 0.008$, $H_2$ from galacturonic acid $P = 0.02$; acetate from glucose $P = 0.0001$, acetate from galacturonic acid $P = 0.0007$). Formate increased under both conditions, but this was not statistically significant on glucose (glucose $P = 0.2$, galacturonic acid $P = 0.0001$). Some changes in acetate production were not significant, possibly due to the use of acetate as an anabolic substrate by the methanogen. Although small concentrations of lactate were sometimes detected (e.g., Table 2), we did not observe lactate formation in these experiments.

Growth rates of NK3A20 on glucose in pure culture and coculture with *M. olleyae* were very similar (Fig. 5). It should be noted that both organisms contribute to optical densities in the cocultures. Interestingly, growth of pure cultures of NK3A20 was fastest with galacturonic acid with added $H_2$ than without, while cocultures with *M. olleyae* grew the slowest. In contrast, on glucose, the cocultures grow most rapidly, and the growth of the NK3A20 pure cultures was slowed when $H_2$ was added. This could suggest that a high partial pressure of $H_2$ was deleterious for growth with glucose but advantageous with galacturonic acid. It is possible that the use of electrons in the first steps of galacturonic acid degradation (catalyzed by the uxaB gene product; Table S4) creates a deficit that is exacerbated by methanogen consumption of $H_2$, and higher $H_2$ concentrations are beneficial for galacturonic acid use. $H_2$ partial pressures in the rumen are typically low (7), and their significance for uronic acid use remains to be determined. Also, the impact of differing uronic acid compositions of ruminant feeds on ruminal $H_2$ and so $CH_4$ formation remains to be determined. In the rumen, where many different sugars are available and used simultaneously, electron use will likely be balanced through the common pools of intracellular intermediates and electron carriers.

Our results agree with previous studies showing end-product shifts in response to interspecies $H_2$ transfer (8, 51, 52). $H_2$ consumption by a hydrogenotrophic microbe in coculture increases the flow of electrons to $H_2$ and probably formate, benefiting the metabolism of the hydrogenogenic microbe by allowing more carbon to flow through the ATP-forming pathway to acetate and less to the formation of other reduced

**TABLE 3** End products of NK3A20 in pure culture, in coculture with *M. olleyae* or in pure culture under a high partial pressure of $H_2$ added at the time of inoculation

| Culture | Substrate[a] | Products (µmol/tube)[b] | | | | | | | Carbon recovery[d] | Available H balance | Dissolved $H_2$ (µM)[e] |
|---|---|---|---|---|---|---|---|---|---|---|---|
| | | Acetate | Butyrate | Formate | Succinate | $H_2$[c] | $CH_4$ | $CO_2$[d] | | | |
| NK3A20 | Glucose | 61.90 ± 1.51 | 59.62 ± 2.70 | 23.42 ± 1.61 | 0.43 ± 0.37 | 186.03 ± 8.50 | 0 | 156.85 | 0.91 | 1.14 | 602 |
| NK3A20 + added $H_2$ | Glucose | 39.50 ± 1.90 | 68.40 ± 4.53 | 27.77 ± 4.16 | 0.90 ± 0.05 | 144.00 ± 3.00 (328.0) | 0 | 146.73 | 0.88 | 1.18 | 1,036 |
| NK3A20 + *M. olleyae* | Glucose | 89.98 ± 17.77 | 39.11 ± 1.79 | 0 | 0.75 ± 0.02 | 0 [242.8] | 60.46 ± 1.11 | 103.22 | 0.84 | 1.20 | 0 |
| NK3A20 | Galacturonate | 96.10 ± 1.33 | 30.90 ± 1.15 | 16.04 ± 0.92 | 0.89 ± 0.21 | 25.40 ± 2.82 | 0 | 140.09 | 0.79 | 1.35 | 82 |
| NK3A20 + added $H_2$ | Galacturonate | 70.23 ± 2.67 | 41.54 ± 1.50 | 28.82 ± 1.07 | 3.43 ± 0.24 | 2.83 ± 6.82 (186.8) | 0 | 117.64 | 0.78 | 1.33 | 578 |
| NK3A20 + *M. olleyae* | Galacturonate | 117.64 ± 7.18 | 14.00 ± 0.80 | 0 | 0.81 ± 0.06 | 0 [102.9] | 25.72 ± 3.80 | 117.84 | 0.73 | 1.39 | 0 |

[a]Initial amount of substrate was 100 µmol/tube.
[b]The values are means from three replicates ± SD.
[c]Values in parentheses are the total final amounts of $H_2$ in experiments where $H_2$ was added at the start of the incubation. Values in square brackets are the inferred amounts of $H_2$ formed calculated from the amounts of $CH_4$ generated.
[d]$CO_2$ produced during pyruvate conversion to acetyl-CoA was included in the carbon balance and was estimated by assuming two $CO_2$ are produced per butyrate and one per acetate. Formate, succinate, and $CH_4$ were then subtracted as one $CO_2$ is used to generate one of each of these products.
[e]Dissolved concentration at end of the experiment, from total $H_2$.
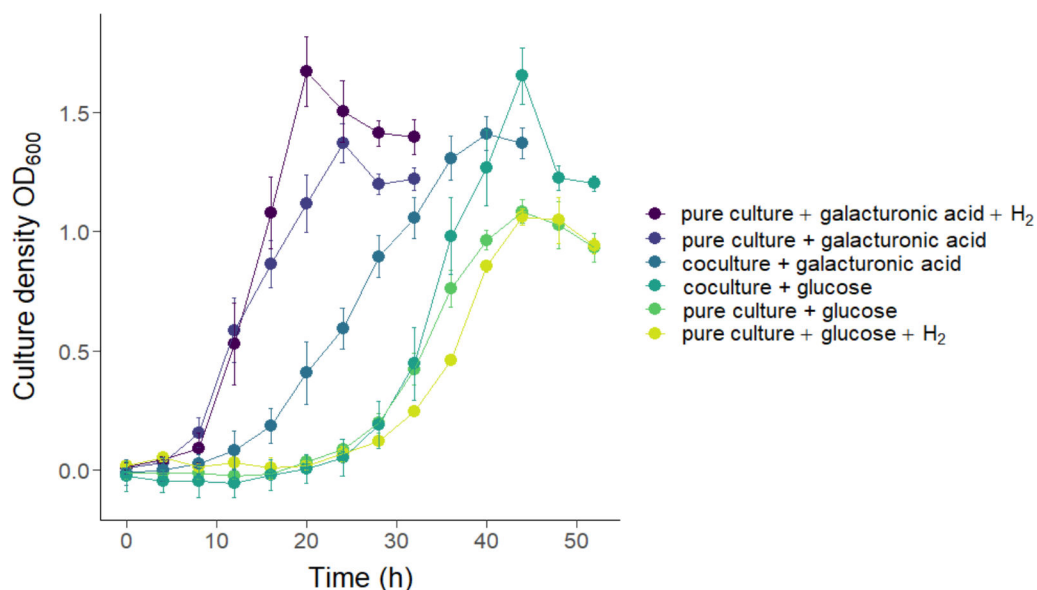
**FIG 5** Growth kinetics of NK3A20 on different substrates, in coculture with *M. olleyae* and alone with or without added $H_2$. Colors represent culture conditions. The values are means from three replicates, and the error bars represent one SD from the mean. Experiments were performed in Hungate tubes.

products like butyrate. Results from pure cultures grown with high partial pressures of $H_2$ demonstrate the opposite impact, where presumably feedback from the high dissolved $H_2$ concentrations limits the formation of $H_2$ and therefore results in the use of those electrons to form butyrate. However, our results with galacturonic acid suggest that while there may be fermentation shifts to produce more $H_2$ in the presence of methanogens, there may be trade-offs for the $H_2$ producer.

## Metabolic predictions from genome

The genome of NK3A20 was analyzed to support experimental findings of substrate use and end-product formation. Fermentation of sugars to pyruvate appears to be through the Embden-Meyerhof-Parnas pathway via glyceraldehyde-3-phosphate, as the genome encodes all the required enzymes (Table S4). Pyruvate and glyceraldehyde-3-phosphate are also produced from uronic acids via 2-dehydro-3-deoxy-phosphogluconate aldolase and 2-dehydro-3-deoxygluconokinase (Table S4). Genes for galacturonic acid and glucuronic acid utilization were present. NK3A20 harbors a large gene cluster (genes G595DRAFT_00078–00103) that contains genes for galacturonic acid metabolism, GH families 28, 35, and 88, pectin methyl esterase (CE8) and predicted ABC oligogalacturonide and arabinogalactan transporters.

The fermentation products observed in the laboratory experiments were supported by genome analyses. NK3A20 possessed genes for pyruvate:ferredoxin oxidoreductase (pyruvate synthase), phosphate acetyltransferase, and acetate kinase, which provide a mechanism for acetate production and reduced ferredoxin formation that presumably leads to $H_2$ generation. Additionally, acetyl-CoA acetyltransferase, 3-hydroxybutyryl-CoA dehydrogenase, enoyl-CoA hydratase, butyryl-CoA dehydrogenase, phosphate transbutyrytransferase, and butyrate kinase were encoded, which form a well-documented pathway to butyrate production, particularly in other *Lachnospiraceae* (53, 54). This pathway acts as an electron sink, recycling reduced cofactors generated during sugar metabolism to acetate. In NK3A20, flow through this pathway increased leading to more butyrate formation and less acetate and $H_2$ (Table 3) when $H_2$ partial pressures were high, and $H_2$ evolution was presumably less favorable. Conversely, butyrate formation was lower when $H_2$ partial pressures were low in the presence of a methanogen.

The genome also encodes a pyruvate formate lyase and its activating enzyme, explaining formate production. A gene encoding lactate dehydrogenase was found in the genome, although lactate was only a trace product under the conditions we used in our experiments. Some succinate was observed in cultures grown with galacturonic acid, and its formation was increased under high $H_2$ partial pressures, but the pathway for formation is not known.

Genes encoding multiple hydrogenase types and hydrogenase expression proteins ( Table S4) were present in the genome. Sequences in the NK3A20 genome encode all subunits of a membrane-associated [NiFe] group 4e hydrogenase, indicating a potential means of $H_2$ production, which is coupled to ferredoxin oxidation (55). Group 4e hydrogenases are also predicted to catalyze the reverse reaction (55). Genes for a putative cytosolic $H_2$ evolving [FeFe] group B hydrogenase were found. The genome also encoded the catalytic and glutamate synthase subunits of a [FeFe] group A2 hydrogenase. Hydrogenase group A2 is uncharacterized, but its association with glutamate synthase has prompted a suggestion that it has a role in nitrogen assimilation (56), although it may have a more general role in $H_2$ generation. This confirms that NK3A20 has mechanisms for reoxidizing reduced electron carriers, like ferredoxin, that are formed during fermentation, and to form $H_2$.

## Potential impact of Rnf, Bcd-Etf, and Ech on ATP yield

A survey of rumen *Lachnospiraceae* genomes in the Hungate 1000 collection showed that many members may possess an electron-bifurcating butyryl-CoA dehydrogenase (Bcd-Etf) (57). This enzyme couples ferredoxin reduction by NADH to crotonyl-CoA reduction to butyryl-CoA (58). Hackmann and colleagues (57) showed that in addition to Bcd-Etf, some *Lachnospiraceae* also possess a transmembrane [NiFe] group 4e hydrogenase (Ech) and an Rnf complex. These complexes oxidize reduced ferredoxin and generate ion gradients that drive ATP synthesis via electron transport phosphorylation. Hypothetically, this could result in the production of up to 4.5 ATP per glucose for fermentation to one butyrate (57, 59) or even 5 ATP per glucose for the production of two acetates (Table S5). The NK3A20 genome encodes all three enzyme complexes.

Estimates of ATP yield indicate that NK3A20 can produce up to 4.35 ATP per glucose in pure cultures, a high yield that is possibly consistent with NK3A20 abundances in microbiome studies (Table 4). This assumes that Ech, and not a cytosolic hydrogenase, is active in all culture conditions. The activity of Rnf may change to accommodate differences in fermentation ratios and maintain relatively consistent ATP yields with different $H_2$ levels. Rnf may be the least active in pure cultures with glucose (Fig. S2A), as approximately all NADH produced during glycolysis should be consumed during fermentation to butyrate. Rnf may be more active in pure cultures with glucose and added $H_2$ (Fig. S2B), as more butyrate is produced, requiring some ferredoxin to be oxidized to produce more NADH. Interestingly, Rnf may operate in reverse in NK3A20 cocultures supplemented with glucose (Fig. S2C), using a small amount of ATP to oxidize NADH and generate sufficient reduced ferredoxin, which is needed by Ech to produce enough $H_2$ to generate the $CH_4$ formed by *M. olleyae*. It is possible that some formate is produced in cocultures, replacing some of the $H_2$, but this would not impact the activity of Rnf, and it would result in a lower ATP yield (57). While overall fermentation product

TABLE 4 Estimated ATP yields from culture conditions in $H_2$ metabolism experiments

| Culture | Substrate | ATP per glucose (using calculated ferredoxin balance) | ATP per glucose (using experimentally determined $H_2$ for Ech) |
|---|---|---|---|
| NK3A20 | Glucose | 4.53 | 4.35 |
| NK3A20 + $H_2$ | Glucose | 4.44 | 4.19 |
| NK3A20 + *M. olleyae* | Glucose | 4.37 | 4.73 |
| NK3A20 | Galacturonate | 3.68 | 3.34 |
| NK3A20 + $H_2$ | Galacturonate | 3.46 | 3.24 |
| NK3A20 + *M. olleyae* | Galacturonate | 3.70 | 3.82 |

trends in cultures with galacturonic acid are similar to those with glucose, ATP yields decrease. Although more carbon is fermented to the high ATP-yielding acetate pathway, this may not compensate for the loss of ATP during galacturonic acid fermentation to pyruvate; the shift away from butyrate may yield less ATP from substrate-level phosphorylation in addition to less ferredoxin from Bcd-Etf (Fig. S3). Though Rnf would still be active in all conditions, less ferredoxin would be available overall, impacting electron transport phosphorylation from Ech. This yields less $H_2$ and, consequently, less ATP.

## Conclusions

Our experiments showed that isolate NK3A20 exhibits flexible metabolisms in response to substrates and $H_2$ partial pressure. The finding that NK3A20 produces significantly less $H_2$, leading to less $CH_4$, when growing with galacturonic acid may prove useful in $CH_4$ mitigation strategies that incorporate feed with higher proportions of uronic acids. The main component of pectin is polygalacturonic acid, and galacturonic acid and other uronic acids are components of other plant components (60). Uronic acids make up <1% on a dry matter basis of grains (61) but are more abundant in grasses and silages (1.5%–4.3%; 62–64) and in grain by-products and various meals (2.2%–3.9%; 61). They can make up quite large parts of some animal feeds, like legumes (2.5%–9.3%; 61, 63, 65, 66), brassicas (up to 15%; 67), and sugar beet pulp (>20%; 68). Future studies could investigate the fermentation profiles of NK3A20 using oligosaccharide substrates and under varying mixed culture conditions (e.g., including a hydrogenotrophic organism and/or an organism that uses lactate to produce propionate or butyrate) to further investigate their relationships to other microbes. The significance of formate as an interspecies electron shuttle is also worthy of investigation. NK3A20 produces formate, but whether is this a major electron sink and the relative significance of $H_2$ and formate remain to be elucidated (69). Additionally, the ATP yields, the metabolic flexibility allowed by the Rnf system, and the expression and functions of the multiplicity of hydrogenases remain to be confirmed and understood.

### AUTHOR AFFILIATIONS

[1]AgResearch Limited, Grasslands Research Centre, Palmerston North, New Zealand
[2]School of Veterinary Science, Massey University, Palmerston North, New Zealand
[3]Riddet Institute, Massey University, Palmerston North, New Zealand

### PRESENT ADDRESS

Nikki Kenters, Ministry of Health, International Affairs, The Hague, Netherlands
Samantha J. Noel, Department of Animal and Veterinary Sciences, AU Viborg – Research Centre Foulum, Aarhus, University, Tjele, Denmark

### AUTHOR ORCIDs

Peter H. Janssen  http://orcid.org/0000-0002-1022-3502

## AUTHOR CONTRIBUTIONS

Rachel A. Kaminsky, Conceptualization, Data curation, Formal analysis, Investigation, Methodology, Visualization, Writing – original draft, Writing – review and editing | Peter M. Reid, Investigation, Writing – original draft | Eric Altermann, Formal analysis, Methodology, Software, Writing – review and editing | Nikki Kenters, Investigation | William J. Kelly, Formal analysis, Writing – original draft, Writing – review and editing | Samantha J. Noel, Investigation, Writing – review and editing | Graeme T. Attwood, Project administration, Resources | Peter H. Janssen, Conceptualization, Funding acquisition, Project administration, Writing – original draft, Writing – review and editing

## DATA AVAILABILITY

The genome of NK3A20 was sequenced as part of the Hungate1000 project (17) at the DOE Joint Genome Institute (JGI GOLD Study ID Gs0033970). The permanent draft is available in IMG (Genome ID 2593339166) and GenBank (BioProject PRJEB16643).

## ADDITIONAL FILES

The following material is available online.

### Supplemental Material

**Supplemental file 1 (AEM00634-23-s0001.docx).** Fig. S1 to S3 and Tables S1 to S5

## REFERENCES

1. McCann JC, Wickersham TA, Loor JJ. 2014. High-throughput methods redefine the rumen microbiome and its relationship with nutrition and metabolism. Bioinform Biol Insights 8:109–125. https://doi.org/10.4137/BBI.S15389
2. Henderson G, Cox F, Ganesh S, Jonker A, Young W, Global Rumen Census Collaborators, Janssen PH. 2015. Rumen microbial community composition varies with diet and host, but a core microbiome is found across a wide geographical range. Sci Rep 5:14567. https://doi.org/10.1038/srep14567
3. Johnson KA, Johnson DE. 1995. Methane emissions from cattle. J Anim Sci 73:2483–2492. https://doi.org/10.2527/1995.7382483x
4. Smith P, Martino D, Cai Z, Gwary D, Janzen H, Kumar P, McCarl B, Ogle S, O'Mara F, Rice C, Scholes B, Sirotenko O, Howden M, McAllister T, Pan G, Romanenkov V, Schneider U, Towprayoon S, Wattenbach M, Smith J. 2008. Greenhouse gas mitigation in agriculture. Philos Trans R Soc Lond B Biol Sci 363:789–813. https://doi.org/10.1098/rstb.2007.2184
5. Lan W, Yang C. 2019. Ruminal methane production: associated microorganisms and the potential of applying hydrogen-utilizing bacteria for mitigation. Sci Total Environ 654:1270–1283. https://doi.org/10.1016/j.scitotenv.2018.11.180
6. Wolin MJ, Miller TL, Stewart CS. 1997. Microbe-microbe interactions, p 467–488. In Hobson PN, TL Miller (ed), The rumen microbial ecosystem, 2nd ed. Chapman and Hall, London, UK. https://doi.org/10.1007/978-94-009-1453-7
7. Janssen PH. 2010. Influence of hydrogen on rumen methane formation and fermentation balances through microbial growth kinetics and fermentation thermodynamics. Anim Feed Sci Technol 160:1–22. https://doi.org/10.1016/j.anifeedsci.2010.07.002
8. Iannotti EL, Kafkewitz D, Wolin MJ, Bryant MP. 1973. Glucose fermentation products in *Ruminococcus albus* grown in continuous culture with *Vibrio succinogenes*: changes caused by interspecies transfer of $H_2$. J Bacteriol 114:1231–1240. https://doi.org/10.1128/jb.114.3.1231-1240.1973
9. Pavlostathis SG, Miller TL, Wolin MJ. 1990. Cellulose fermentation by continuous cultures of *Ruminococcus albus* and *Methanobrevibacter smithii*. Appl Microbiol Biotechnol 33:109–116. https://doi.org/10.1007/BF00170581

10. Ntaikou I, Gavala HN, Kornaros M, Lyberatos G. 2008. Hydrogen production from sugars and sweet sorghum biomass using *Ruminococcus albus*. Int J Hydrog Energy 33:1153–1163. https://doi.org/10.1016/j.ijhydene.2007.10.053

11. Zheng Y, Kahnt J, Kwon IH, Mackie RI, Thauer RK. 2014. Hydrogen formation and its regulation in *Ruminococcus albus*: involvement of an electron-bifurcating [FeFe]-hydrogenase, of a non-electron-bifurcating [FeFe]-hydrogenase, and of a putative hydrogen-sensing [FeFe]-hydrogenase. J Bacteriol 196:3840–3852. https://doi.org/10.1128/JB.02070-14

12. Greening C, Geier R, Wang C, Woods LC, Morales SE, McDonald MJ, Rushton-Green R, Morgan XC, Koike S, Leahy SC, Kelly WJ, Cann I, Attwood GT, Cook GM, Mackie RI. 2019. Diverse hydrogen production and consumption pathways influence methane production in ruminants. ISME J 13:2617–2632. https://doi.org/10.1038/s41396-019-0464-2

13. Williams AG, Withers SE, Joblin KN. 1994. The effect of cocultivation with hydrogen-consuming bacteria on xylanolysis by *Ruminococcus flavefaciens*. Curr Microbiol 29:133–138. https://doi.org/10.1007/BF01570753

14. Chen M, Wolin MJ. 1977. Influence of $CH_4$ production by *Methanobacterium ruminatum* on the fermentation of glucose and lactate by *Selenomonas ruminatum*. Appl Environ Microbiol 34:756–759. https://doi.org/10.1128/aem.34.6.756-759.1977

15. Bauchop T, Mountfort DO. 1981. Cellulose fermentation by a rumen anaerobic fungus in both the absence and the presence of rumen methanogens. Appl Environ Microbiol 42:1103–1110. https://doi.org/10.1128/aem.42.6.1103-1110.1981

16. Marvin-Sikkema FD, Richardson AJ, Stewart CS, Gottschal JC, Prins RA. 1990. Influence of hydrogen-consuming bacteria on cellulose degradation by anaerobic fungi. Appl Environ Microbiol 56:3793–3797. https://doi.org/10.1128/aem.56.12.3793-3797.1990

17. Seshadri R, Leahy SC, Attwood GT, Teh KH, Lambie SC, Cookson AL, Eloe-Fadrosh EA, Pavlopoulos GA, Hadjithomas M, Varghese NJ, Paez-Espino D, Hungate1000 project collaborators, Perry R, Henderson G, Creevey CJ, Terrapon N, Lapebie P, Drula E, Lombard V, Rubin E, Kyrpides NC, Henrissat B, Woyke T, Ivanova NN, Kelly WJ. 2018. Cultivation and sequencing of rumen microbiome members from the Hungate1000 collection. Nat Biotechnol 36:359–367. https://doi.org/10.1038/nbt.4110

18. Schmidt O, Wüst PK, Hellmuth S, Borst K, Horn MA, Drake HL. 2011. Novel [NiFe]- and [FeFe]-hydrogenase gene transcripts indicative of active facultative aerobes and obligate anaerobes in earthworm gut contents. Appl Environ Microbiol 77:5842–5850. https://doi.org/10.1128/AEM.05432-11

19. Biddle A, Stewart L, Blanchard J, Leschine S. 2013. Untangling the genetic basis of fibrolytic specialization by *Lachnospiraceae* and *Ruminococcaceae* in diverse gut communities. Diversity 5:627–640. https://doi.org/10.3390/d5030627

20. Meehan CJ, Beiko RG. 2014. A phylogenomic view of ecological specialization in the *Lachnospiraceae*, a family of digestive tract-associated bacteria. Genome Biol Evol 6:703–713. https://doi.org/10.1093/gbe/evu050

21. Henderson G, Yilmaz P, Kumar S, Forster RJ, Kelly WJ, Leahy SC, Guan LL, Janssen PH. 2019. Improved taxonomic assignment of rumen bacterial 16S rRNA sequences using a revised SILVA taxonomic framework. PeerJ 7:e6496. https://doi.org/10.7717/peerj.6496

22. McLoughlin S, Spillane C, Claffey N, Smith PE, O'Rourke T, Diskin MG, Waters SM. 2020. Rumen microbiome composition is altered in sheep divergent in feed efficiency. Front Microbiol 11:1981. https://doi.org/10.3389/fmicb.2020.01981

23. Kenters N, Henderson G, Jeyanathan J, Kittelmann S, Janssen PH. 2011. Isolation of previously uncultured rumen bacteria by dilution to extinction using a new liquid culture medium. J Microbiol Methods 84:52–60. https://doi.org/10.1016/j.mimet.2010.10.011

24. Button DK, Schut F, Quang P, Martin R, Robertson BR. 1993. Viability and isolation of marine bacteria by dilution culture: theory, procedures, and initial results. Appl Environ Microbiol 59:881–891. https://doi.org/10.1128/aem.59.3.881-891.1993

25. Rea S, Bowman JP, Popovski S, Pimm C, Wright A-DG. 2007. *Methanobrevibacter millerae* sp. nov. and *Methanobrevibacter olleyae* sp. nov., methanogens from the ovine and bovine rumen that can utilize formate for growth. Int J Syst Evol Microbiol 57:450–456. https://doi.org/10.1099/ijs.0.63984-0

26. Coico R. 2005. Gram staining. Curr Protoc Microbiol Appendix 3:A–3C. https://doi.org/10.1002/9780471729259.mca03cs00

27. Askenova HY, Rainey FA, Janssen PH, Zavarzin GA, Morgan HW. 1992. *Spirochaeta thermophila* sp. nov., an obligately anaerobic, polysaccharolytic, extremely thermophilic bacterium. Int J Syst Evol Microbiol 42:175–177. https://doi.org/10.1099/00207713-42-1-175

28. Wilhelm E, Battino R, Wilcock RJ. 1977. Low-pressure solubility of gases in liquid water. Chem Rev 77:219–262. https://doi.org/10.1021/cr60306a003

29. Battino R. 1984. The Ostwald coefficient of gas solubility. Fluid Phase Equilib 15:231–240. https://doi.org/10.1016/0378-3812(84)87009-0

30. Richardson AJ, Calder AG, Stewart CS, Smith A. 1989. Simultaneous determination of volatile and non-volatile acidic fermentation products of anaerobes by capillary gas chromatography. Lett Appl Microbiol 9:5–8. https://doi.org/10.1111/j.1472-765X.1989.tb00278.x

31. Gottschalk G. 1986. Bacterial metabolism. Springer, New York, NY. https://doi.org/10.1007/978-1-4612-1072-6

32. R Core Team. 2021. R: a language and environment for statistical computing. R Foundation for Statistical Computing, Vienna, Austria.

33. Wickham H. 2016. ggplot2: elegant graphics for data analysis. Springer-Verlag, Cham. https://doi.org/10.1007/978-3-319-24277-4

34. Wickham H. 2007. Reshaping data with the reshape package. J Stat Soft 21:1–20. https://doi.org/10.18637/jss.v021.i12

35. Wickham H. 2011. The split-apply-combine strategy for data analysis. J Stat Soft 40:1–29. https://doi.org/10.18637/jss.v040.i01

36. Garnier S, Ross N, Rudis R, Camargo AP, Sciaini M, Scherer C. 2021. Rvision-colorblind-friendly color maps for R. R package version 0.6.1

37. Parte AC, Sardà Carbasse J, Meier-Kolthoff JP, Reimer LC, Göker M. 2020. List of prokaryotic names with standing in nomenclature (LPSN) moves to the DSMZ. Int J Syst Evol Microbiol 70:5607–5612. https://doi.org/10.1099/ijsem.0.004332

38. Kumar S, Stecher G, Li M, Knyaz C, Tamura K, Battistuzzi FU. 2018. MEGA X: molecular evolutionary genetics analysis across computing platforms. Mol Biol Evol 35:1547–1549. https://doi.org/10.1093/molbev/msy096

39. Jukes TH, Cantor CR. 1969. Evolution of protein molecules, p 21132. In Munro HN (ed), Mammalian protein metabolism. Academic Press, New York, NY.

40. Chen I-MA, Chu K, Palaniappan K, Ratner A, Huang J, Huntemann M, Hajek P, Ritter S, Varghese N, Seshadri R, Roux S, Woyke T, Eloe-Fadrosh EA, Ivanova NN, Kyrpides NC. 2021. The IMG/M data management and analysis system v.6.0: new tools and advanced capabilities. Nucleic Acids Res 49:D751–D763. https://doi.org/10.1093/nar/gkaa939

41. Altermann E, Lu J, McCulloch A. 2017. GAMOLA2, a comprehensive software package for the annotation and curation of draft and complete microbial genomes. Front Microbiol 8:346. https://doi.org/10.3389/fmicb.2017.00346

42. Rutherford K, Parkhill J, Crook J, Horsnell T, Rice P, Rajandream MA, Barrell B. 2000. Artemis: sequence visualization and annotation. Bioinformatics 16:944–945. https://doi.org/10.1093/bioinformatics/16.10.944

43. Kanehisa M, Sato Y, Morishima K. 2016. BlastKOALA and GhostKOALA: KEGG tools for functional characterization of genome and metagenome sequences. J Mol Biol 428:726–731. https://doi.org/10.1016/j.jmb.2015.11.006

44. Søndergaard D, Pedersen CNS, Greening C. 2016. HydDB: a web tool for hydrogenase classification and analysis. Sci Rep 6:34212. https://doi.org/10.1038/srep34212

45. Clarridge JE. 2004. Impact of 16S rRNA gene sequence analysis for identification of bacteria on clinical microbiology and infectious diseases. Clin Microbiol Rev 17:840–862. https://doi.org/10.1128/CMR.17.4.840-862.2004

46. Everett KD, Bush RM, Andersen AA. 1999. Emended description of the order *Chlamydiales*, proposal of *Parachlamydiaceae* fam. nov. and *Simkaniaceae* fam. nov., each containing one monotypic genus, revised taxonomy of the family *Chlamydiaceae*, including a new genus and five new species, and standards for the identification of organisms. Int J Syst Bacteriol 49:415–440. https://doi.org/10.1099/00207713-49-2-415

47. Parks DH, Chuvochina M, Rinke C, Mussig AJ, Chaumeil P-A, Hugenholtz P. 2022. GTDB: An ongoing census of bacterial and archaeal diversity through a phylogenetically consistent, rank normalized and complete genome-based Taxonomy. Nucleic Acids Res 50:D785–D794. https://doi.org/10.1093/nar/gkab776

48. Pallen MJ, Rodriguez-R LM, Alikhan N-F. 2022. Naming the unnamed: over 65,000 *Candidatus* names for unnamed *Archaea* and *Bacteria* in the genome taxonomy database. Int J Syst Evol Microbiol 72:005482. https://doi.org/10.1099/ijsem.0.005482

49. Palevich N, Kelly WJ, Leahy SC, Denman S, Altermann E, Rakonjac J, Attwood GT. 2019. Comparative genomics of rumen *Butyrivibrio* spp. uncovers a continuum of polysaccharide-degrading capabilities. Appl Environ Microbiol 86:e01993-19. https://doi.org/10.1128/AEM.01993-19

50. Vahidi MF, Gharechahi J, Behmanesh M, Ding X-Z, Han J-L, Hosseini Salekdeh G. 2021. Diversity of microbes colonizing forages of varying lignocellulose properties in the sheep rumen. PeerJ 9:e10463. https://doi.org/10.7717/peerj.10463

51. Vogels GD, Hoppe WF, Stumm CK. 1980. Association of methanogenic bacteria with rumen ciliates. Appl Environ Microbiol 40:608–612. https://doi.org/10.1128/aem.40.3.608-612.1980

52. Rotaru A-E, Shrestha PM, Liu F, Ueki T, Nevin K, Summers ZM, Lovley DR. 2012. Interspecies electron transfer via hydrogen and formate rather than direct electrical connections in cocultures of *Pelobacter carbinolicus* and *Geobacter sulfurreducens*. Appl Environ Microbiol 78:7645–7651. https://doi.org/10.1128/AEM.01946-12

53. Miller TL, Jenesel SE. 1979. Enzymology of butyrate formation by *Butyrivibrio fibrisolvins*. J Bacteriol 138:99–104. https://doi.org/10.1128/jb.138.1.99-104.1979

54. Vacca M, Celano G, Calabrese FM, Portincasa P, Gobbetti M, De Angelis M. 2020. The controversial role of human gut *Lachnospiraceae*. Microorganisms 8:573. https://doi.org/10.3390/microorganisms8040573

55. Greening C, Biswas A, Carere CR, Jackson CJ, Taylor MC, Stott MB, Cook GM, Morales SE. 2016. Genomic and metagenomic surveys of hydrogenase distribution indicate $H_2$ is a widely utilised energy source for microbial growth and survival. ISME J 10:761–777. https://doi.org/10.1038/ismej.2015.153

56. Calusinska M, Happe T, Joris B, Wilmotte A. 2010. The surprising diversity of clostridial hydrogenases: a comparative genomic perspective. Microbiology 156:1575–1588. https://doi.org/10.1099/mic.0.032771-0

57. Hackmann TJ, Firkins JL. 2015. Electron transport phosphorylation in rumen butyrivibrios: unprecedented ATP yield for glucose fermentation to butyrate. Front Microbiol 6:622. https://doi.org/10.3389/fmicb.2015.00622

58. Li F, Hinderberger J, Seedorf H, Zhang J, Buckel W, Thauer RK. 2008. Coupled ferredoxin and crotonyl-coenzyme A (CoA) reduction with NADH catalyzed by the butyryl-CoA dehydrogenase/Etf complex from *Clostridium kluyveri*. J Bacteriol 190:843–850. https://doi.org/10.1128/JB.01417-07

59. Buckel W, Thauer RK. 2013. Energy-conservation via electron bifurcating ferredoxin reduction and proton/Na+ translocating ferredoxin oxidation. Biochim Biophys Acta 1827:94–113. https://doi.org/10.1016/j.bbabio.2012.07.002

60. Fry SC. 2011. Cell wall polysaccharide composition and covalent crosslinking. Annu Plant Rev 41:1–42. https://doi.org/10.1002/9781444391015

61. Knudsen KEB. 1997. Carbohydrate and lignin contents of plant materials used in animal feeding. Anim Feed Sci Technol 67:319–338. https://doi.org/10.1016/S0377-8401(97)00009-6

62. Waite R, Gorrod ARN. 1959. The structural carbohydrates of grasses. J Sci Food Agric 10:308–317. https://doi.org/10.1002/jsfa.2740100603

63. Bourquin LD, Fahey GC. 1994. Ruminal digestion and glycosyl linkage patterns of cell wall components from leaf and stem fractions of alfalfa, orchardgrass, and wheat straw. J Anim Sci 72:1362–1374. https://doi.org/10.2527/1994.7251362x

64. Bica R, Palarea-Albaladejo J, Lima J, Uhrin D, Miller GA, Bowen JM, Pacheco D, Macrae A, Dewhurst RJ. 2022. Methane emissions and rumen metabolite concentrations in cattle fed two different silages. Sci Rep 12:5441. https://doi.org/10.1038/s41598-022-09108-w

65. Barahona R, Lascano CE, Narvaez N, Owen E, Morris P, Theodorou MK. 2003. *In vitro* degradability of mature and immature leaves of tropical forage legumes differing in condensed tannin and non-starch polysaccharide content and composition. J Sci Food Agric 83:1256–1266. https://doi.org/10.1002/jsfa.1534

66. Shang H, Li R, Wu H, Sun Z. 2019. Polysaccharides from *Trifolium repens* L. extracted by different methods and extraction condition optimization. Sci Rep 9:6353. https://doi.org/10.1038/s41598-019-42877-5

67. Jørgensen H, Knudsen KEB, Lauridsen C. 2012. Influence of different cultivation methods on carbohydrate and lipid compositions and digestibility of energy of fruits and vegetables. J Sci Food Agric 92:2876–2882. https://doi.org/10.1002/jsfa.5755

68. Hindrichsen IK, Wettstein H-R, Machmüller A, Soliva CR, Bach Knudsen KE, Madsen J, Kreuzer M. 2004. Effects of feed carbohydrates with contrasting properties on rumen fermentation and methane release *in vitro*. Can J Anim Sci 84:265–276. https://doi.org/10.4141/A03-095

69. Leahy SC, Janssen PH, Attwood GT, Mackie RI, McAllister TA, Kelly WJ. 2022. Electron flow: key to mitigating ruminant methanogenesis. Trends Microbiol 30:209–212. https://doi.org/10.1016/j.tim.2021.12.005